The Effects of Polydispersity on the Morphology of Polystyrene-Polyferrocenyldimethylsilane Block Copolymer Thin Films

by

Joy C. Perkinson

Submitted to the Department of Materials Science and Engineering
in Partial Fulfillment of the Requirements for the Degree of
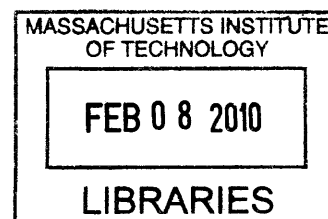
Bachelor of Science

at the

Massachusetts Institute of Technology

May 2009

[June 2009]

Signature of Author: _____
Department of Materials Science and Engineering
May 8, 2009

Certified by: _____
Caroline A. Ross
Professor of Materials Science and Engineering
Thesis Supervisor

Accepted by: _____
Lionel C. Kimerling
Professor of Materials Science and Engineering
Chair, Undergraduate Committee

1

Acknowledgements

I would like to deeply thank my advisor, Professor Caroline A. Ross, for accepting me into her research group for three consecutive years, and for acting as a mentor throughout my studies of magnetism and polymers. Without her guidance, this thesis would not have been written.

I would like to thank Vivian Peng-Wei Chuang and Filip Ilievski for teaching me how to conduct research in a laboratory setting. They taught me the techniques that made my research possible.

I would like to thank MIT, my alma mater, for teaching me the skills to work under pressure. The abilities that MIT has granted me will last a lifetime. They ensured I kept a level head throughout the week before this thesis was due.

I would like to thank the MIT Assassins' Guild and American Jiu Jitsu for keeping my head clear.

I would like to thank all mentors and role models who have helped me along my way. In particular, and in order of appearance: Annabeth Jensen, Robert Salazar, Jeffrey Payne, Art Leo, Arthur Glasfeld, Peter Child, and Berit Johannes. Whether or not you know it, you have all inspired me to make more of myself.

Most of all, I would like to give my sincerest thank you to my family, as well as to VKC and SJW, for supporting me throughout my time at MIT. You have made me who I am today.

To all listed above: live long and prosper.

Contents

1 Introduction

1.1 Motivation

As the size of electronic and magnetic devices decreases, nanoscale patterning becomes an increasingly important area of research. Two different approaches have been taken to pattern media: top-down methods such as lithography, and bottom-up methods such as self-assembly. Top-down assembly methods have the advantages of precision and accuracy, but are hard to scale for certain industrial applications due to their low throughput. Self-assembly methods are more easily scalable for applications requiring mass production. Thus, self-assembly has attracted attention and is an area of ongoing research for its potential to create high-throughput, periodic nanoscale patterns.

Block copolymers are a class of commonly-studied materials for nanoscale self-assembly. Block copolymers are long molecules that consist of "blocks" of chemically differing polymers attached end-to-end. Under the right conditions, these blocks will phase separate, spontaneously forming periodic microdomains. Diblock copolymers, which have only two blocks, have been found to form a variety of well-ordered morphologies with nanoscale periodicity (Figure 1) [1].
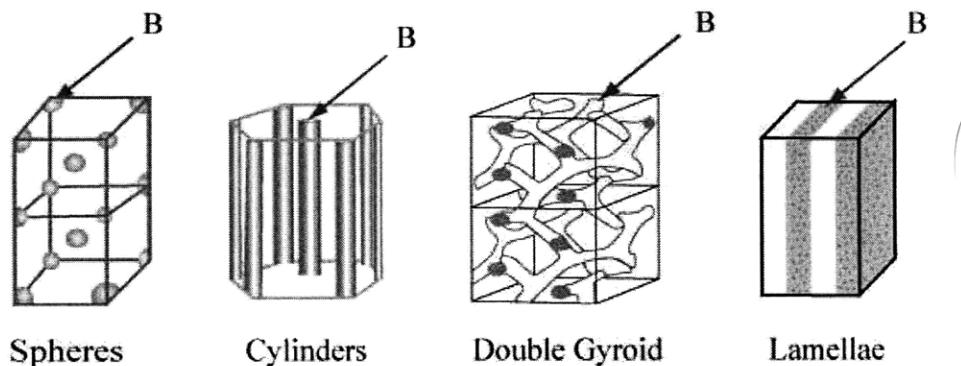

Spheres   Cylinders   Double Gyroid   Lamellae

Figure 1: The ordered structures formed by diblock copolymers [2].

Nanoscale patterning is of particular interest for use in high-density magnetic data storage. Thin films of diblock copolymers can serve as self-assembled templates for patterning magnetic materials [3]. The morphology of block copolymers is generally predicted using a χN diagram. These diagrams plot the dependence of phase transitions on polymer volume fraction and the value χN (Figure 2) [1]. In these diagrams,
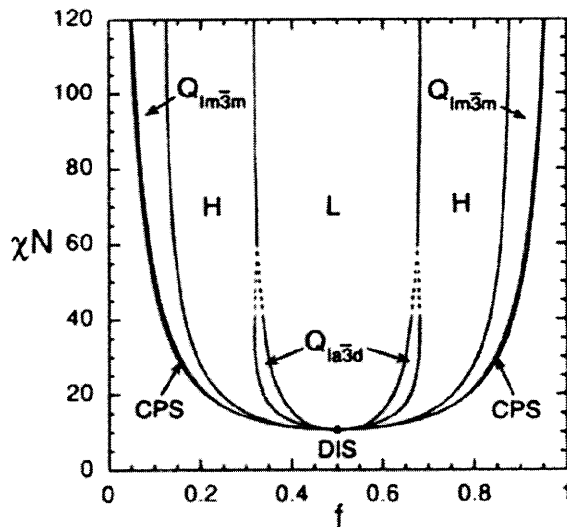

Figure 2: The generic χN diagram for block copolymer systems, showing the dependence of phase transitions and the order-disorder transition on volume fraction and the χN value of the system. In this diagram, CPS is the order-disorder transition, $Q_{Im\bar{3}m}$ is the spherical regime, H is the cylindrical regime, $Q_{Ia\bar{3}a}$ is the double gyroid regime, and L is the lamellar regime [4].

volume fraction is on the horizontal axis, and χN is on the vertical axis. N refers to the degree of polymerization of the entire chain, and χ is the Flory-Huggins interaction parameter used to describe the enthalpic interactions between the two blocks. The full expression for χ is:

$$\chi_{12} = \frac{z}{k_B T}\left(\varepsilon_{12} - \tfrac{1}{2}(\varepsilon_{11} + \varepsilon_{22})\right)$$

where z is the number of adjacent lattice sites used in the Flory-Huggins derivation of free energy, $k_B T$ is the thermal energy, and the ε terms are the interaction energies

5

between the two species present in diblock copolymer systems. Interaction energies are negative, with more negative indicating a more enthalpically favorable interaction. Thus, a positive value of χ indicates unfavorable enthalpic interactions between the two blocks, and thus a tendency for the blocks to phase separate. A negative value of χ indicates favorable interactions between the two blocks. This expression has been simplified for the PS/PFS system [5]:

$$\chi(T) = 0.028 + 3.28/T$$

This equation takes into account the interaction energies between the PS and PFS blocks. T is the annealing temperature in Kelvin. χN can thus be calculated for the samples in this study given the annealing temperature and degree of polymerization of the samples. This value can be used to predict the morphology of diblock copolymer thin films.

Once the desired morphology has been attained, the block copolymers can serve as lithographic masks. These masks can be used to etch into magnetic materials to create periodic magnetic nanoparticles to be used as bits for data storage. The spherical morphology block copolymers researched in this study exhibit periodicity around 30nm, which would pack data at around 1×10^{13} particles/in^2, over a terabyte of information per square inch. This amount of information density, along with the high throughput of self-assembly methods, makes block copolymers an attractive choice for nanoscale patterning of high-density magnetic data storage devices as well as other electronic, optic, and magnetic devices.

One of the limitations of using thin polymer films as lithographic masks is their relatively high etch rate, in comparison to magnetic materials, during reactive ion etching (RIE). RIE is a form of plasma etching used to selectively remove materials or to transfer patterns. When used for transferring patterns from a polymer film

6

into a substrate, RIE needs to etch the material below the polymer film before the polymer is etched away completely. Some magnetic materials used for data storage applications, such as cobalt and nickel, cannot be etched by RIE but require ion beam etching. Thus, attempting to transfer the pattern directly from a polymer film to a cobalt film would etch away the polymer without affecting the cobalt layer. However, this problem can be solved using a combination of more complex processing methods and organometallic polymers, which are highly etch-resistant. When organic-organometallic block copolymers are used in thin films, the organic block can be easily etched away, leaving the organometallic structures for use in pattern transfer [6]. By designing block copolymers with organometallic materials as the minority block, one can create highly etch-resistant organometallic spheres within an organic matrix that can be easily removed via RIE [7]. In this way, one can create lithographic masks with periodic spherical morphology that is etch-resistant enough to be used in the processing for magnetic data storage applications.

The organic-organometallic block copolymer used in this study is polystyrene-*block*-polyferrocenyldimethylsilane (PS-*b*-PFS) (Figure 3) [8]. At the volume fractions
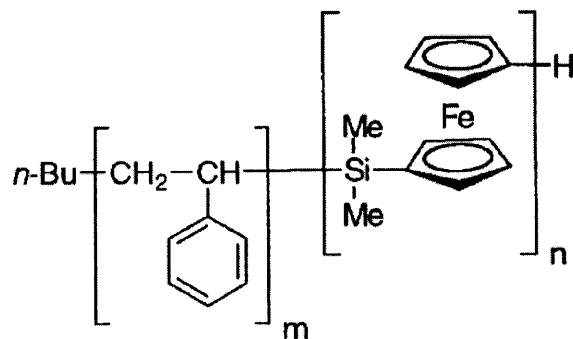

Figure 3: The chemical structure of polystyrene-*block*-polyferrocenyldimethylsilane [9].

investigated, the organometallic PFS block forms mostly spheres, though cylinders

7

are occasionally observed. The PFS spheres sit within a matrix of PS, and a brush layer of PFS forms atop the silicon substrate (Figure 4). The number of layers of
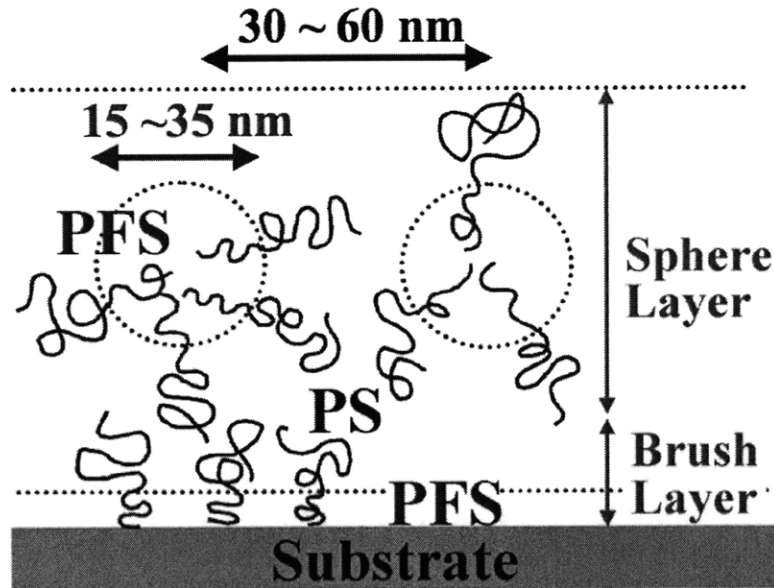

Figure 4: A side view of the PS/PFS thin film morphology. PFS forms spheres within a matrix of PFS, and a brush layer of PFS forms atop the substrate. The number of layers of PFS spheres can be controlled by adjusting the film thickness [10].

PFS spheres can be controlled by adjusting the thickness of the polymer film, though for pattern transfer applications, a monolayer is ideal.

While PFS spheres are relatively etch-resistant for a polymer, they are still not able to resist ion beam etching long enough to transfer a pattern directly into a magnetic material. A method was devised to circumvent this problem by transferring the pattern into increasingly etch-resistant materials [3]. In this method, the PS/PFS film is deposited onto a layered stack. The PS is etched away, and the PFS is used as a mask to transfer the pattern into the top layer, silicon dioxide, via RIE. This pattern is then etched with RIE into the next layer, tungsten. Layers are etched down with RIE and ashing until only a periodic array of tungsten dots remains above the

magnetic layer. Finally, the pattern is transferred to a magnetic material, such as cobalt, via ion beam etching (Figure 4). The resulting nanoparticles can be used as
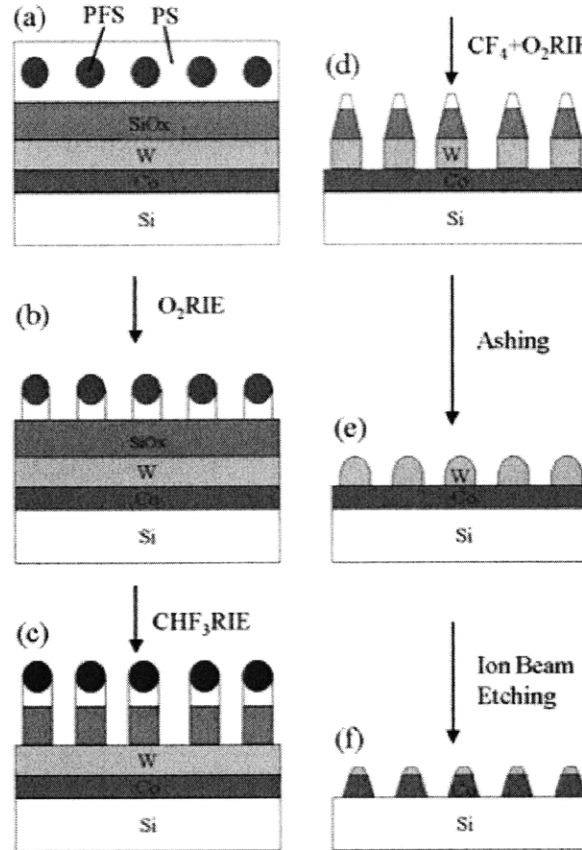
Figure 4: The layer-by-layer pattern transfer method. A PS/PFS film is deposited on a layered substrate. Layers are etched through via RIE, ashing, and ion beam etching, and the pattern is eventually transfered into a layer of cobalt, creating magnetic nanodots [3].

bits in high-density data storage.

1.2   Purpose

In order to effectively use self-assembled structures as templates for data storage devices, both the spacing and size of surface features must be uniform. Extensive research has been done to control the packing of polymer spheres and to remove the

9

"grain boundaries" that can form in packed sphere structures using templated self-assembly methods to induce ordering by topographical and/or chemical patterns [10]. However, some discussions of sphere uniformity blame poor uniformity on polydispersity effects [11, 12].

Polydispersity is quantified using the polydispersity index (PDI), which is defined as

$$PDI = M_w/M_n$$

where M_w is the weight average molar mass of the polymer and M_n is the number average molar mass of the polymer:

$$M_w = \sum N_i M_i^2 / \sum N_i M_i \qquad \textit{Weight-average molar mass}$$

$$M_n = \sum N_i M_i / \sum N_i \qquad \textit{Number-average molar mass}$$

In these expressions, N_i is the number of molecules with given molar mass M_i. By definition, $M_w \geq M_n$, so the minimum PDI of any polymer sample is PDI = 1. This value indicates perfect uniformity, in which all molecules have exactly the same molecular weight. High PDI values indicate a wide range of molecular weights within a sample.

This study aims to determine the extent to which PDI affects the morphology of PFS microdomains. Five PS/PFS block copolymers were prepared by collaborators at University Twente in the Netherlands, each with a different PDI between 1.109 and 1.198. However, the polymers also varied in molecular weight and PFS volume fraction. Thus, the end result of this research is a discussion of the relative effects of varying PDI, volume fraction, and molecular weight at the same time. Sample annealing time and film thickness effects are also discussed.

2 Experimental Procedure

Polymers with varying PDI, molecular weight, and PFS volume fraction were fabricated by collaborators at University Twente (Table 1). Their methods of fabrication

Table 1: Physical properties of the five PS/PFS samples studied. Φ indicates volume fraction.

Sample	Φ PFS vol %	MW_{total} (g/mol)	MW_{PS} (g/mol)	MW_{PFS} (g/mol)	PDI
A	19	54125	42597	11866	1.109
B	17	48282	38639	9445	1.114
C	22	47127	35098	11866	1.123
D	20	51202	39501	12060	1.188
E	13	50529	42113	7502	1.198

are included as Appendix A [13].

To prepare the polymers for deposition on a substrate, 1.5wt% solutions of PS/PFS in toluene were created. The solutions were left to sit for at least 2 hours to allow the polymer to dissolve and ensure a homogeneous solution. Then, prime silicon wafer was cut into pieces around a square centimeter in size. These pieces of silicon were cleaned with a nitrogen gun in MIT's NanoStructures Laboratory (NSL) cleanroom facilities. Then, polymer solution was deposited onto the wafer pieces via spin coating. The speed of the spin coater was set prior to polymer deposition, to ensure reproducible results. Samples were spun for 60 seconds at a range of spin speeds. Film thickness was controlled by adjusting the spin speed, with higher speeds corresponding to thinner films. Spin speeds ranging from 1500 to 6000 RPM corresponded to film thicknesses between 32 and 63nm. For samples not specifically investigating the effects of film thickness, films around 42nm were used, created at a spin speed of 3000 RPM. This thickness was chosen because it corresponded to a single monolayer of PFS microdomains for all five polymers.

Deposited films were taken to CMSE facilities for annealing. Samples were annealed at 140°C (413 K) in a vacuum furnace. This temperature is above the glass transition temperature for both PS and PFS, so their mobility was substantially increased during annealing. This allowed the block copolymers to rearrange into organized, periodic arrays. Most samples were annealed for 24-30 hours, though annealing times from 1 to 7 days were investigated. The ovens were then vented with nitrogen gas, and samples were transported back to NSL cleanroom facilities for imaging. Before imaging, RIE was used to run a 25-second oxygen plasma etch at 90W. This step removed the top layer of PS matrix so PFS features could be observed. Finally, samples were imaged using scanning probe microscopy (SEM).

Properties of the PFS features observed in the SEM images were analyzed using image processing and MATLAB software. The PFS microdomains were targeted using a threshold overlay in SigmaScan, an image analysis program, and their areas and coordinates were recorded. MATLAB scripts (Appendix B) were used to calculate object areas, calculate distances between objects, and create pair density functions (PDFs) for each sample. Together, the scripts calculated the mean and standard deviation for both the area of PFS microdomains and the distance between them. The PDF, $g(r)$, is a dimensionless measure of the density of objects around a point, and is defined as

$$g(r) = \frac{1}{\rho} \frac{dn(r, r+dr)}{dA(r, r+dr)}$$

where ρ is the areal particle density, dn is the number of pairs of particles between a radial distance r and $r + dr$, and dA is the area contained between r and $r + dr$. Periodic PDFs that decay quickly indicate short range order (Figure 6), while periodic PDFs that do not decay over a large distance indicate long-range order. The correlation length, ξ, was determined by recording the distance at which the
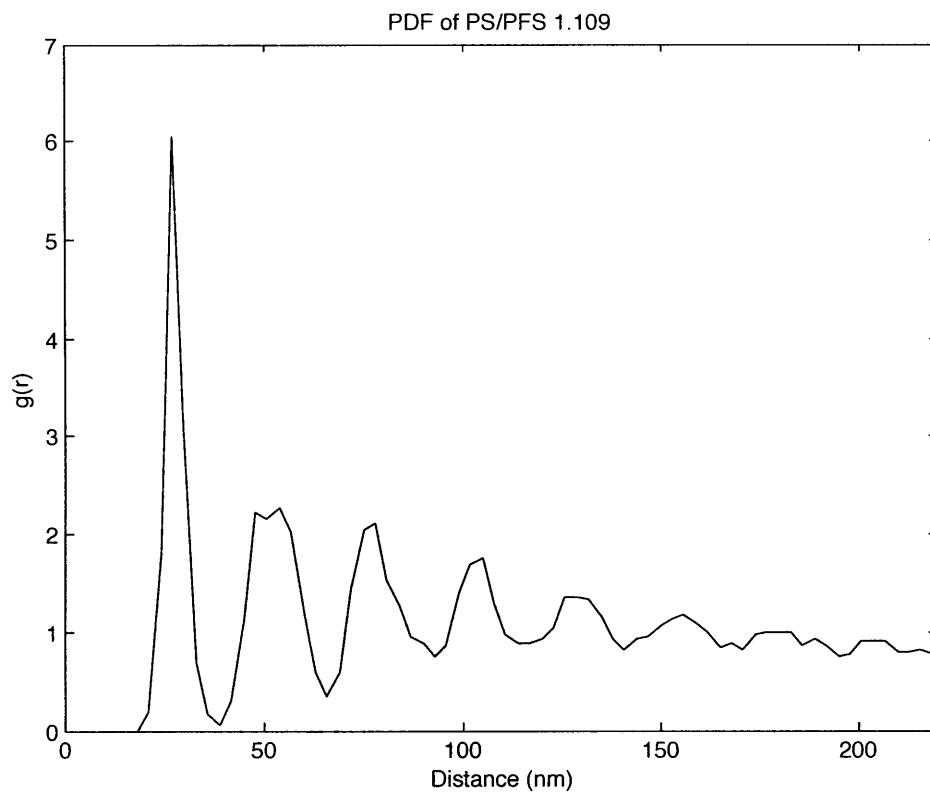
Figure 6: A pair density function for PS/PFS with PDI 1.109 and thickness 42nm. The decaying oscillations indicate short range order.

amplitude of PDF oscillations fell below 5% of the peak amplitude.

3 Results and Discussion

3.1 Volume Fraction

Volume fraction was found to have a significant impact on the observed morphology of the PS/PFS films. At low volume fractions ($\Phi_{PFS} = 13\%$), the PFS microdomains are small and irregular. At mid-range volume fractions ($\Phi_{PFS} = 17 - 19\%$), the PFS microdomains are regular spheres. At higher volume fractions ($\Phi_{PFS} = 20 - 22\%$), PFS cylinders begin to form in the matrix of spheres (Figure 7). The emergence of
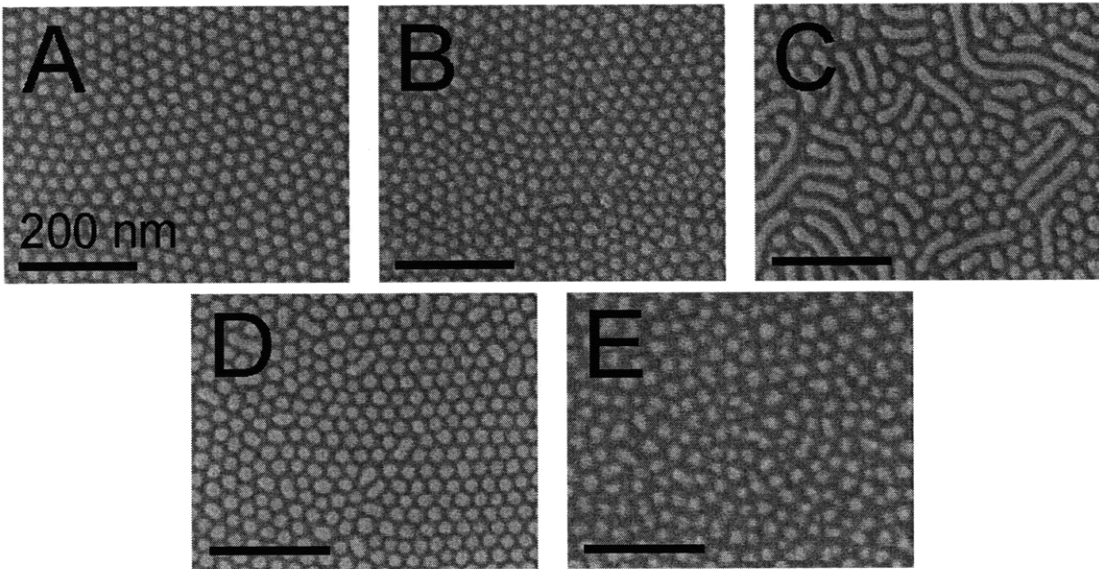

Figure 7: The effects of volume fraction on PS/PFS films with thickness 42nm. PFS volume fractions are (A) 19%, (B) 17%, (C) 22%, (D) 20%, and (E) 13%. Lettering corresponds to the sample lettering from Table 1. Sample E, with PFS volume fraction of $\phi = 13\%$, is near the order-disorder transition, and is thus irregular. Samples A and B are in the spherical phase. Cylinders begin appearing in sample D, with $\phi = 20\%$. In sample C, with $\phi = 22\%$, many cylinders are visible. These transitions are consistent with the χN diagram describing diblock copolmyer morphology.

cylinders at $\Phi_{PFS} = 20\%$ is similar to results from previous work [3, 14].

As revealed by comparing the volume fractions of samples A-E (Table 1) with the

calculated data for those samples (Table 2), there is a strong correlation between vol-

Table 2: Data on the 42nm-thick films of the five PS/PFS samples.

Sample	Φ PFS vol %	Area (nm)		Distance (nm)		ξ (nm)
		Mean	Std. Dev	Mean	Std. Dev	
A	19	249.8	44.9	29.5	3.1	171
B	17	222.5	47.7	26.4	2.9	141
C	22	447.1	381.2	30.3	3.2	135
D	20	290.7	104.9	29.0	3.3	195
E	13	117.8	47.3	22.7	4.5	120

ume fraction and both the mean area of PFS features and the mean distance between them. The trend of increasing mean area values corresponds directly to increasing volume fraction. This is also true of mean distance values, with the minor exception of mean distances 29.0 and 29.5nm corresponding to 20 and 19% PFS instead of the other way around. These data are consistent with the emergence of spheres and then cylinders as PFS volume fraction increases, as these regime changes increase both the area of PFS microdomains and the distance between them. The sample with the lowest volume fraction, 13%, exhibits the lowest mean area, lowest mean distance, and largest standard distance deviation of any of the samples, corresponding to the small and irregularly-shaped PFS microdomains in the sample. The sample with the highest volume fraction, 22%, exhibits the highest mean area, standard area deviation, and mean distance between PFS microdomains of any sample, indicating the presence of large cylinders. These two samples also exhibit the lowest correlation lengths of any samples, indicating that they are furthest from the uniform spherical domain. This result can be verified by observing SEM images of the films (Figure 7).

The sphere-to-cylinder (S/C) transition is generally predicted using the χN diagram. We can calculate the χN value of our samples using the annealing temperature and degree of polymerization. χ depends on the annealing temperature, which

is 140°C (410 K) for these samples.

$$\chi_{PS/PFS}(T) = 0.028 + 3.28/T$$

$$\chi_{PS/PFS}(410) = 0.028 + 3.28/410$$

$$= 0.036$$

We can calculate the degree of polymerization N for our polymers using the molecular weight of the blocks and the molar masses of the monomers. Through these calculations, it is found that the average degree of polymerization for the polymers is $N = 422.4$. χN is therefore 16.6 for our polymers.

This value can be used to compare the observed morphology of the PS/PFS samples to the morphology predicted by the χN diagram in Figure 2. The χN diagram predicts that samples with a χN value of 16.6 will exhibit a S/C transition at approximately 28% PFS. While no samples in this study have volume fractions large enough to observe a complete transition into the cylindrical domain, the emergence of short cylinders at 20% PFS and the mix of spheres and cylinders at 22% PFS suggest that a complete S/C transition will occur close to 28% PFS.

However, the χN diagram also predicts that a volume fraction of 13% PFS in a sample with a χN value of 16.6 will be disordered. This prediction is significantly different than the observed morphology of PFS microdomains at that volume fraction. While the microdomains in the sample with volume fraction 13% are less ordered than the microdomains observed at higher volume fractions, PS/PFS phase separation is observed. This result can be explained by the fact that the generic χN diagram is designed for bulk systems, not for thin films. The phase behavior of thin films is different than that of bulk block copolymers due to a variety of factors, such as the preferential interaction of different blocks with the substrate. Surface energy terms,

16

which are more pronounced in thin films, could also affect the phase behavior of the system.

3.2 Thickness

Six film thicknesses were investigated for sample A, ranging from 36.1 to 62.2nm. A significant change in properties occurred between 45.0 and 48.9nm (Table 3). The

Table 3: Properties of PS/PFS films with varying thickness. A significant change in properties is observed between 45.0 and 48.9nm, corresponding to the formation of a second layer of PFS spheres above 45nm.

Thickness (nm)	Area (nm)		Distance (nm)		ξ (nm)
	Mean	Std. Dev	Mean	Std. Dev	
62.2	223.5	81.7	29.8	3.6	165
53.7	221.4	69.1	29.4	3.6	138
48.9	213.7	57.3	28.8	3.3	162
45.0	274.0	47.1	29.8	2.7	195
39.3	265.1	68.4	31.2	3.4	189
36.1	260.7	72.1	31.5	3.7	162

mean area of PFS microdomains increased sharply, from 213.7 to 274.0nm. This change can be attributed to the formation of a second layer of PFS features at thicknesses greater than 45nm. Below 45nm, there is a monolayer of PFS spheres, in addition to the brush layer of PFS at the substrate. Above 45nm, a bilayer of PFS spheres can be seen (Figure 8). The data exhibit some correlation with the two thickness regimes. The mean area of PFS microdomains in the bilayer is between 213.7 and 223.5nm, while the mean area in the monolayer is between 260.7 and 274.0nm. Within these regimes, data indicate that mean area decreases slightly as film thickness decreases. However, the mean area variation within the bilayer regime exhibits a variation of only 4.6% of the total microdomain area, while the variation within the monolayer regime exhibits a variation of only 5.1%. These variations are small
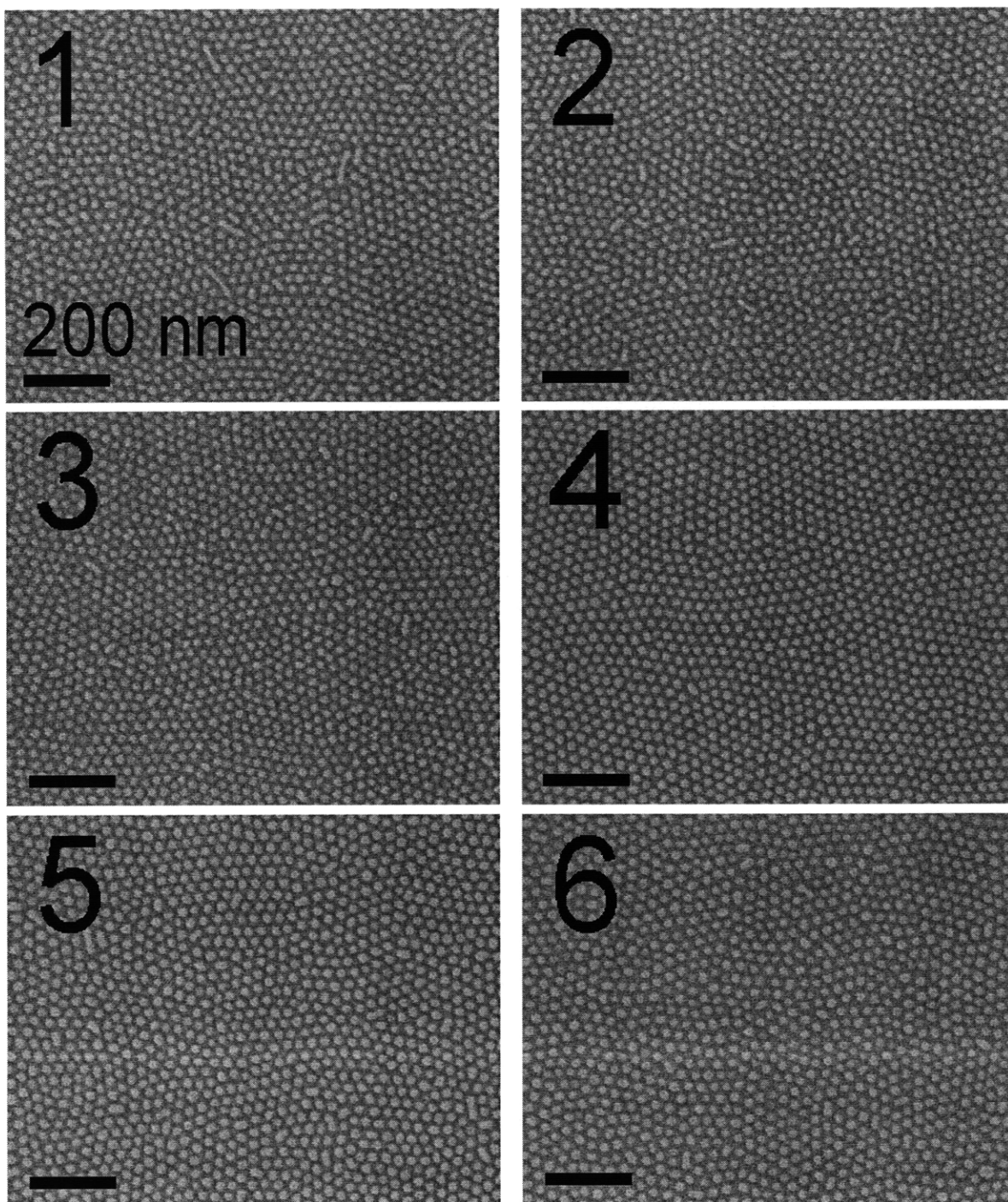
Figure 8: The effects of film thickness on PFS microdomains. Thicknesses are (1) 62.2nm, (2) 53.7nm, (3) 48.9nm, (4) 45.0nm, (5) 39.3nm, and (6) 36.1nm. Two layers of PFS spheres are visible above 45nm. At 45nm and below, a monolayer is observed.

enough that they could be within the range of experimental error. The existence of two thickness regimes is reflected in the other data as well. The mean distance between PFS microdomains is generally larger in the monolayer samples, and the standard deviation of both mean area and distance is generally smaller. Furthermore, the correlation lengths of the monolayer samples are larger than those of the bilayer. Together, these results indicate that monolayer films of PFS spheres exhibit greater uniformity, longer-range order, and greater spacing between microdomains than bilayer films. These results reflect the greater conformational entropy present in systems with multiple layers of spheres.

3.3   Annealing Time

The effects of annealing time were investigated for a film of sample A. Samples were annealed at 140°C for 1, 2, 4, and 7 days (Figure 9). The films showed increased uniformity as annealing time increased (Table 4). The sample annealed for 1 day

Table 4: Properties of films with varying annealing times, made from 42nm thick PS/PFS sample A with PDI 1.109.

Annealing	Area (nm)		Distance (nm)		ξ
time (days)	Mean	Std. Dev	Mean	Std. Dev	(nm)
1	247	61.6	26.1	8.4	135
2	245	66.5	26.2	8.7	198
4	273	48.6	29.8	3.0	156
7	274	44.0	29.8	2.6	198

contained some PFS cylinders, the sample annealed for 2 days contained fewer, and by 4 days of annealing, no more were observed and the PFS spheres were spaced evenly.

Though some changes were observed with annealing time, the changes were small.
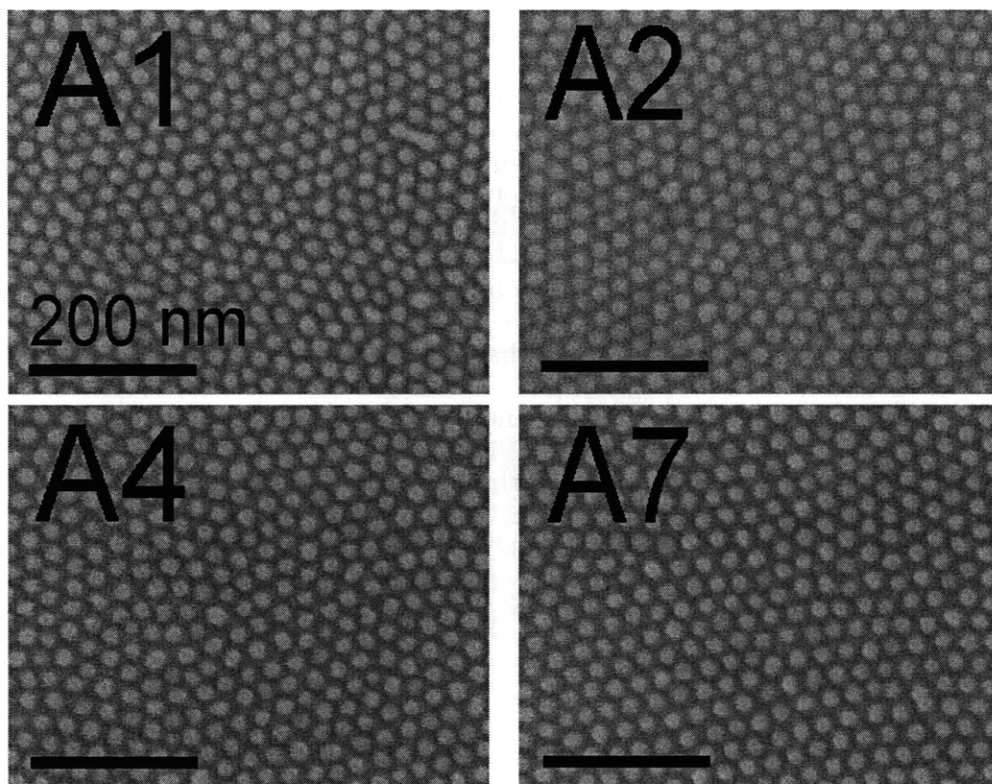
Figure 9: The effects of annealing time on PS/PFS films with thickness 42nm. Samples were annealed at 140°C for (A1) 1 day, (A2) 2 day, (A4) 4 day, (A7) 7 days.

However, the large increase in correlation length between the first and second days of annealing, from 135 to 198nm, indicates increased uniformity after the first day of annealing. Furthermore, the absence of cylinders at longer annealing times qualitatively indicates that most of the self-organizing occurs within the first two days of annealing.

3.4 Molecular Weight

The total polymer molecular weight was not found to correlate strongly with the observed structure of the films (Tables 1, 2). However, increased molecular weight should increase the mean area of microdomains and the distance between them. For

the samples in this study, the effects of molecular weight could be outweighed by the effects of volume fraction. Samples A and D have similar volume fraction, and thus provide the best opportunity for examination of molecular weight effects. Sample A has PFS volume fraction 19%, while sample D has PFS volume fraction 20%. Based on volume fraction effects alone, sample D should exhibit greater mean area and distance, and greater standard deviation. However, sample A has a higher molecular weight than sample D. The samples have a total molecular weight of 54125 and 51202 g/mol, respectively. While the mean PFS microdomain area, standard area deviation, and standard distance deviation of sample D are greater than that of sample A, sample D exhibits a lower mean distance between microdomains than sample A. While the mean distance values are very close together, at 29.5 and 29.0nm respectively, these values are the only discrepancy in a mean area and distance trend that strictly increases with volume fraction. The discrepancy could be due to larger molecules increasing the spacing between PFS microdomains.

Other than this small discrepancy in mean distance data, no correlation is observed between the data and molecular weight. However, larger molecules should increase the area of microdomains and the spacing between them. It is expected that if a wider range of molecular weights were represented in the the study, molecular weight effects on morphology would be observed.

3.5   Polydispersity

The PDI was found to have no noticeable effect on the observed morphology (Tables 1, 2). While PDI has been used to justify variations in morphology in some studies [11, 12], this study shows no correlation between changes in PDI and surface features. Samples A, C, and E have PDI 1.109, 1.123, and 1.198 respectively. However,

the mean area of the PFS microdomains in sample A is 249.8nm, which increases to 447.1nm for sample C, and then decreases to 117.8nm for sample E. The standard area deviation of these three samples are 44.9, 381.2, and 47.3nm, respectively. The mean distance between PFS microdomains for the samples are 29.5, 30.3, and 22.7nm, respectively. Though samples A, C, and E span the range of polydispersities investigated in this study, they exhibit no trend for mean area, mean distance, or standard area deviation. Similarly, the correlation length for the sample with PDI 1.109 is 171nm, which increases to 195nm for the sample with PDI 1.188, and decreases to 120nm for the sample with PDI 1.198. The only observed trend is in the standard distance deviation. Overall, the standard deviation of distances between microdomains increases with PDI. However, the variance is small. The standard distance deviations of the samples with PDI 1.109, 1.114, 1.123, and 1.188 vary only by tenths, a change of less than 5% the total standard deviation value. Additionally, the sample with PDI 1.114 contradicts this trend by exhibiting the lowest standard distance deviation while not having the lowest PDI. Thus, the only observed trend is relatively weak.

These results can be explained by considering the number of chains in each PFS microdomain. The density of PFS is 1.26 g/cm^3 (Appendix A). PFS spheres have a cross-sectional area around 250nm^2, corresponding to a radius of 8.92nm, and a total sphere volume of 2.97μm. Combining the PFS density and the sphere volume, and using an approximate molar weight of 10,000g/mol for the PFS block, the total number of chain ends per sphere is

$$2.97 \times 10^{-18} cm^3 \left(\frac{1.26g}{cm^3} \right) \left(\frac{1mol}{10,000g} \right) \left(\frac{6.022 \times 10^{23} chains}{1mol} \right) \approx 224 \; chains/sphere$$

If this calculation is repeated twice, once using conservative estimates of all the quantities and once using generous estimates, the range of values for the number of chains per sphere is

$$144 < \frac{chains}{sphere} < 424$$

For a microdomain with N chains, the average variation in number of chains goes as $\sqrt{N}$. Thus, an average variation of $\pm$ 15 chains per sphere is expected for the PFS microdomains in this study. Using the generous and conservative estimates of the number of chains per sphere, the expected variation in number of chains per microdomain is calculated between 12 and 21 PFS chains. For the mid-range estimate, the expected variation is a 7% change. This value is low enough that the effects of variations in the number of chains per sphere are not easily observable. For this reason, the variations in PDI do not correlate with observed properties of the films.

4 Conclusion

Thin films of organic-organometallic block copolymers such as polystyrene-*block*-polyferrocenyldimethylsilane (PS/PFS) have been investigated as self-assembled lithographic masks for nanoscale patterning of highly etch-resistant magnetic materials. For magnetic data storage applications, microdomain uniformity is required in order for data to be easily read and written. This study examined the relative importance of five polymer properties on the morphology of PS/PFS thin films. In particular, this study investigated the effects of polydispersity (PDI), which has been cited as having a significant effect on block copolymer morphology.

The effects of varying volume fraction, film thickness, annealing time, molecular weight, and PDI were investigated in terms of mean PFS microdomain area, standard deviation of area, mean distance between PFS microdomains, standard deviation of distance, and correlation length, as well as qualitative analysis of SEM images. Of the polymer properties, volume fraction was found to have the greatest effect on PS/PFS morphology. This result can be explained by the χN phase diagram for block copolymer morphology. Thickness variations were found to cause a significant change in mean microdomain area during the transition from a PFS sphere monolayer to a bilayer. Annealing time analysis revealed that samples reached equilibrium after approximately 2 days of annealing. Molecular weight was found to have a negligible effect on PS/PFS morphology. Finally, PDI was found to have no noticeable effect on the morphology of PS/PFS microdomains. This result can be explained by calculating that the average number of PFS chains per microdomain is 224, and the variance between spheres is approximately 15, a change of only 7%. Thus, in relation to the other polymer properties investigated in this study, PDI has a negligible effect on PS/PFS thin film morphology.

A   Polymer Fabrication Methods

Written by Janet Acikgoz [13].

N,N,N',N',-Tetramethylethylenediamine (TMEDA), ferrocene, styrene, *n*-butyllithium (1.6 M in hexanes), dibutylmagnesium (1.0 M in heptane) and dichlorodimethylsilane were purchased from Aldrich. [1]Dimethlysilaferrocenophane was prepared as described earlier and was purified by sequential crystallization and vacuum sublimation cycles [14, 15]. Crystallizations were performed at low temperature in *n*-heptane. Solutions of styrene in ethylbenzene were dried on dibutylmagnesium and distilled under vacuum. *n*-Butyllithium was diluted to 0.2 M with *n*-heptane, which was dried over *n*-butyllithium and distilled under vacuum. Tetrahydrofuran (THF) for anionic polymerizations was distilled from sodium-benzophenone under argon, degassed in three freeze-pump-thaw cycles, and distilled by vacuum condensation from n-butyllithium at low temperature.

Poly(styrene-*block*-ferrocenyldimethylsilane) copolymers were synthesized by sequential anionic polymerization carried out in an Mbraun Labmaster 130 glovebox under an atmosphere of prepurified nitrogen (<0.1 ppm of H_2O). Polymerization of styrene in ethylbenzene was initiated by *n*-butyllithium and stirred for 5 hours at room temperature. After the styrene block formation was completed, [1]dimethlysilaferrocenophane was added to the solution followed by some THF, allowing the formation of the organometallic block. After 2 hours, the living chains were terminated by adding a few drops of degassed methanol. The polymers were precipitated in methanol and dried under vacuum. Variation in polydispersity of the copolymers was achieved by adding the required amount of initiator in several portions at different time intervals, rather than at once.

The polymers were characterized by gel permeation chromatography (GPC) and

^{1}H NMR spectrometry. GPC measurements were carried out in THF using Waters[TM] microstyragel columns with pore sizes of $10^5, 10^4, 10^3 \mathring{A}$ and a 500 $\mathring{A}$ guard column (Waters). The instrument was equipped with a dual detection system consisting of a differential refractometer (Waters model 410) and a viscometer (Viscotek model H502). Molar masses were determined relative to narrow polystyrene standards. ^{1}H NMR spectra were recorded on a Varian Unity Inova (300 MHz) instrument at 300.3 MHz in deuterated chloroform. Block ratios were calculated from ^{1}H NMR peak integrals. The density of poly(ferrocenyldimethylsilane), 1.26 g/cm^3, was obtained using a pycnometer.

B MATLAB Code

B.1 Area Data

Mean area and standard deviation were calculated using the MATLAB program *AreaHist*. Inputs to the code were *filename*, the name of the data text file created by SigmaScan, *numbuckets*, the number of buckets to include in the area data histogram, and *PDI* and *rpm*, the PDI of the polymer sample and the spin speed used. The latter two inputs were used in the title of the area data histogram. Outputs of the code were a histogram of area data (Figure B-1), and an output message of the
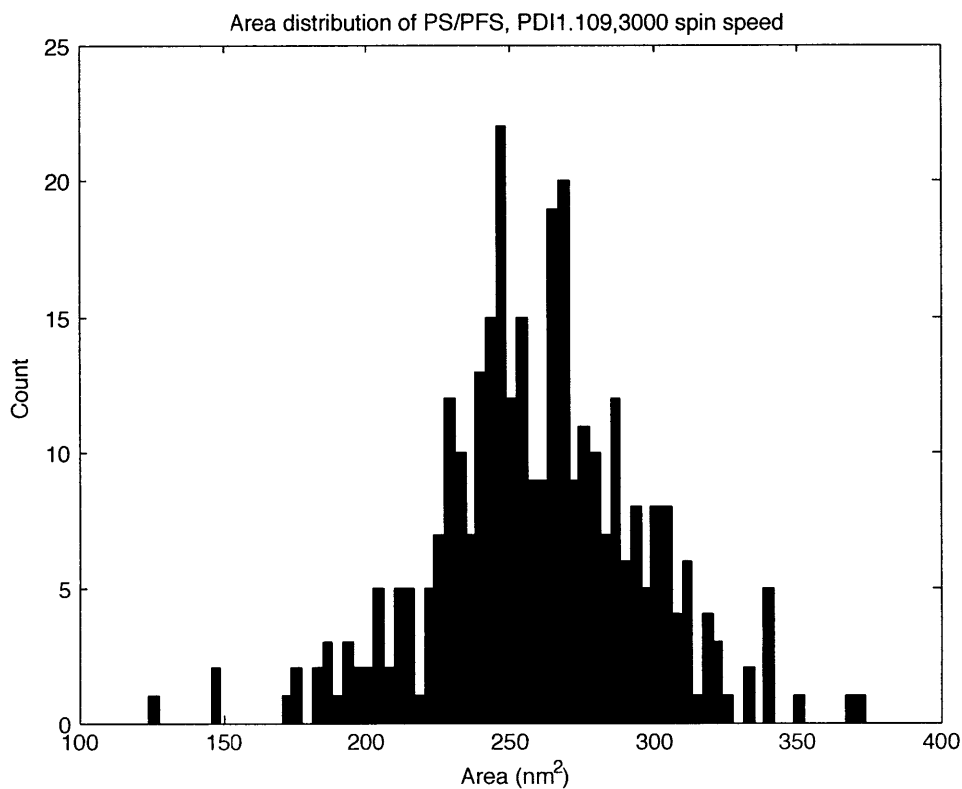

Figure B-1: A sample histogram of areas produced by the MATLAB script *AreaHist*. These data were created for the sample with PDI 1.109, spin speed 3000, and film thickness 43nm.

number of areas plotted, the mean area of all PFS microdomains in the sample, and the standard deviation for the area data.

AreaHist was prepared with the help of Mark Mascaro [16], and the code is displayed below.

```
function areahistdata = AreaHist(filename, numbuckets, PDI, rpm)

file = fopen(filename);
unparsedarray = fscanf(file, '%f %f %f');
% First column of unparsedarray is areas
% Second and third columns are distances

N=1;
for i=1:(length(unparsedarray)/3)
    for j=1:3
        areaarray(i,j) = unparsedarray(N);
        N = N + 1;
    end
end

% Next, gather the areas

areahistdata = areaarray(:,1);

disp('Number of areas plotted: ')
disp(length(areahistdata))

    [mean,stddev] = normfit(areahistdata);
    disp('mean = '); disp(mean)
    disp('std dev = '); disp(stddev)

hist(areahistdata,numbuckets);
title(strcat('Area distribution of PS/PFS', ', PDI ', PDI, ', ', rpm, ...
    ' spin speed'));
xlabel('Area (nm^2)'); ylabel('Count');
```

B.2 Distance Data

Distance data were calculated using two programs in series, *DistHist* and *Gauss*. *DistHist* creates a histogram of the distances between all pairs of PFS microdomains (Figure B-2a). This amount of data is difficult to visually process, but the axes can be adjusted to zoom in on the histogram to view the first peak (Figure B-2b). The distance that marks the end of the first peak must be recorded for use as an input to the *Gauss* function. The output of *DistHist* is an array of the distance data plotted in the histogram. This output must be stored as a local variable, for use in the *Gauss* function.

Gauss calculates the mean distance and standard deviation between nearest neighbor PFS microdomains. *Gauss* takes inputs *distances*, the data output from the *DistHist* function, *endofpeak*, the distance at which the first peak of the distance histogram ended, *PDI*, the PDI of the sample, and *rpm*, the spin speed at which the sample was created. The input *endofpeak* is important because, for nearest-neighbor data, only the first peak from the distance histogram should be analyzed. *Gauss* displays a plot of the analyzed distance peak (Figure B-3) and prints the mean distance and standard deviation between nearest-neighbor PFS microdomains. Code for *DistHist* and *Gauss* is shown below.
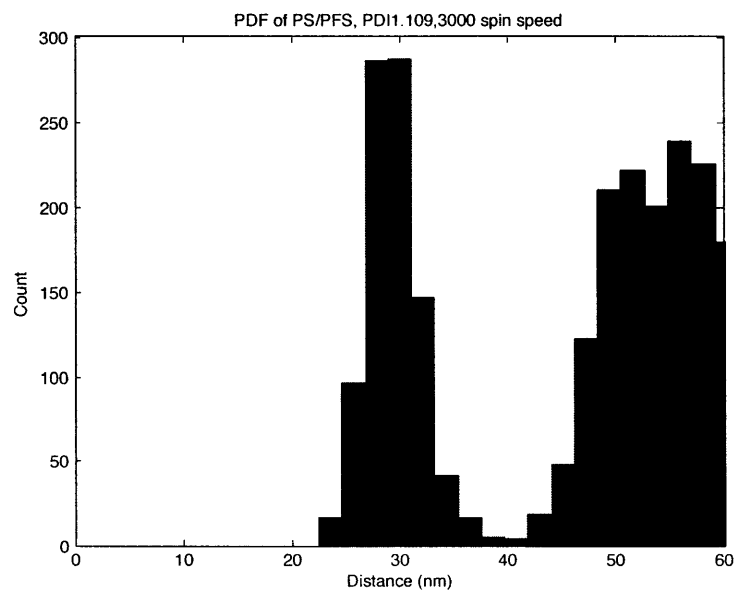
DistHist:

```
function disthistdata=PDF(filename, numbuckets, PDI, rpm)

file = fopen(filename);
unparseddistancearray = fscanf(file, '%f %f %f');
% First column of distancearray is areas;
% second column is x values,
% third column is y-values
N=1;
for i=1:(length(unparseddistancearray)/3)
    for j=1:3
```

PDF of PS/PFS, PDI1.109,3000 spin speed

(a)

PDF of PS/PFS, PDI1.109,3000 spin speed
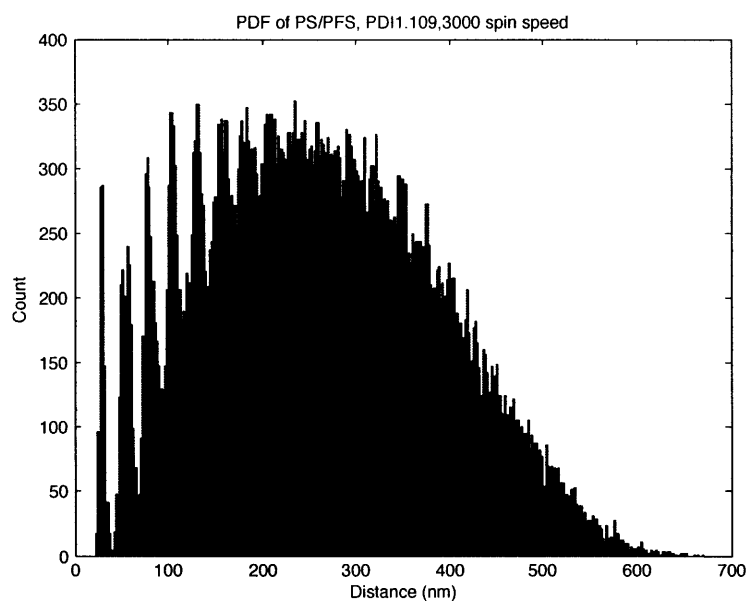
(b)

Figure B-2: (a) A histogram of the distances between PFS microdomains in a sample with PDI 1.109 and thickness 42nm, created by the MATLAB script *DistHist*. (b) A closer view of the first peak, showing the end of the first peak at ~ 40nm. The value for the end of the peak is an input for *Gauss*, the MATLAB function that calculates the mean distance and standard deviation values used in this study.
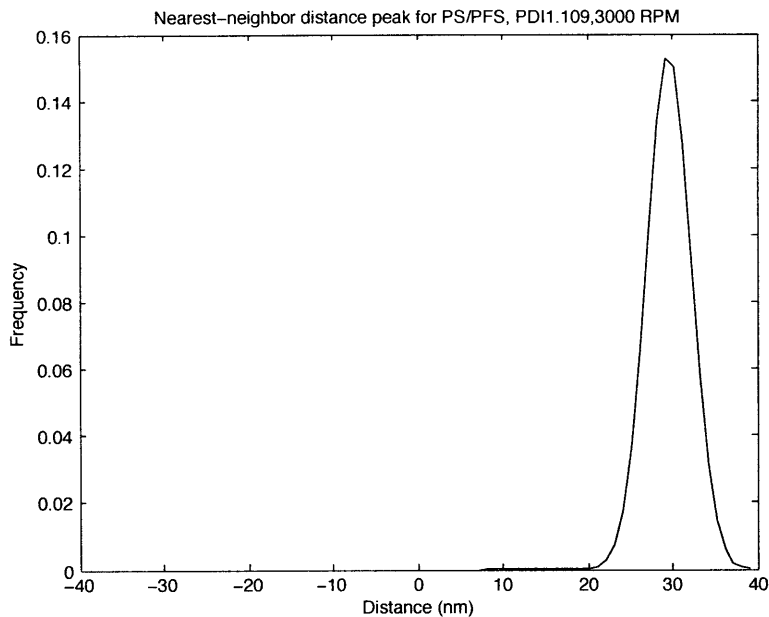
Figure B-3: The nearest-neighbor distance peak plotted and analyzed by the MAT-LAB function *Gauss*. *Gauss* uses this peak to calculate the mean nearest-neighbor distance and standard deviation.

```
        distancearray(i,j) = unparseddistancearray(N);
        N = N + 1;
    end
end

% Gather the distances
datalength = length(distancearray(:,1));
disthistdata = zeros(((datalength)^2 - datalength)/2,1);


N=1;
for i=1:(datalength-1)
    for j=(i+1):datalength
        xdist = distancearray(i,2) - distancearray(j,2);
        ydist = distancearray(i,3) - distancearray(j,3);
        dist = sqrt(xdist.^2 + ydist.^2);
        disthistdata(N) = dist;
        N = N + 1;
    end
end
```

31

```
% Plot
hist(disthistdata,numbuckets);
title(strcat('PDF of PS/PFS', ', PDI ', PDI,', ', rpm,' spin speed'));
xlabel('Distance (nm)'); ylabel('Count');
```

Gauss:

```
function Gauss(distances, endofpeak, PDI, rpm)

firstpeak = distances(find(distances<endofpeak));

[mean,stddev] = normfit(firstpeak);
disp('mean = '); disp(mean)
disp('std dev = '); disp(stddev)

% Plot the Gaussian
xgrid = [stddev-(endofpeak-stddev):1:endofpeak];
plot(xgrid, normpdf(xgrid, mean, stddev),'black');
title(strcat('Nearest-neighbor distance peak for PS/PFS, PDI ', PDI,...
    ', ',rpm,' RPM'));
xlabel 'Distance (nm)'
ylabel 'Frequency'
```

B.3 Pair Density Function

The pair density functions (PDFs) were generated using the MATLAB program *PDF*. *PDF* takes three inputs, *filename*, the name of the file from which to import the data, *imagesize*, the area of the image in nm^2, and *dr*, a value controlling the granularity of the final image. Using these inputs, *PDF* calculates the pair density function, *g(r)*:

$$g(r) = \frac{1}{\rho} \frac{dn(r,r+dr)}{dA(r,r+dr)}$$

The code for *PDF*, shown below, was prepared with significant help from Mark Mascaro [16].

```
function PDF(filename, imagesize, dr)

% imagesize is in nm^2

disp('Importing file.')

file = fopen(filename);
UDA = fscanf(file, '%f %f %f');
%UDA = Unparsed Distance Array
%First column of distancearray is areas;
%second column is x values,
%third column is y-values

disp('File opened. Parsing positions.')

N=1;
PDA = zeros(length(UDA)/3,3);
for i=1:(length(UDA)/3)
    for j=1:3
        PDA(i,j) = UDA(N);
        N = N + 1;
    end
end

disp('Locations parsed. Calculating distances.')

%LET'S MAKE SOME RADII
listofdistances = zeros(length(PDA)^2/2-length(PDA),1);
N=1;
for i=1:(length(PDA))
    for j=i+1:(length(PDA))
        if (i ~= j)
            listofdistances(N) = sqrt((PDA(i,2)-PDA(j,2))^2 +...
                (PDA(i,3)-PDA(j,3))^2);
            N=N+1;
        end
    end
end

disp('Distances calculated!')

density = length(PDA)/imagesize;
```

```
r=[0:dr:max(listofdistances)];
g = zeros(length(r),1);
for i = 1:length(r)
    g(i) = length(find((listofdistances>r(i)) &...
        (listofdistances<(r(i)+dr))))/(density*pi*((r(i)+dr)^2-r(i)^2));
end
%g = length(find((listofdistances>r) &
%(listofdistances<(r+dr)))) ./(density*pi*((r+dr).^2-r.^2));

plot(r,g,'black')
axis([0 300 0 1000])
```

References

[1] F.S. Bates and G.H. Fredrickson, *Annu. Rev. Phys. Chem.* **41**, 525-557 (1990).

[2] MIT Open Courseware, 3.063, Spring 2007. Retrieved May 2009.

[3] J.Y. Cheng, C.A. Ross, C.Z.-H. Chan, E.L. Thomas, R.G.H. Lammertink, and G.J. Vancso, *Adv. Mater.* **13** (15), 1174-1178 (2001).

[4] R.G.H. Lammerink, *Poly(ferrocenyldimethylsilanes) at the Interface of Chemistry and Materials Science: Synthesis, Structure-Properties and Thin Film Applications*. Enschede: Print Partners Ipskamp, 2000.

[5] H.B. Eitouni, N.P. Balsara, H. Hahn, J.A. Pople, and M.A. Hempenius, *Macromolecules* **35** (20), 7765-7772 (2002).

[6] G.N. Taylor, T.M. Wolf, and L.E. Stillwagon, *Solid State Technol.* **27**, 145-155 (1984).

[7] R.G.H. Lammertink, M.A. Hempenius, V.Z.H. Chan, E.L. Thomas, G.J. Vancso, *Chem. Mater.* **13**, 429 (2001).

[8] P. Nguyen, P. Gómez-Elipe, and I. Manners, *Chem. Rev.* **99**, 1515-1548 (1999).

[9] J.Y. Cheng. *Fabrication and Characterization of Nanostructures from Self-assembled Block Copolymers*. Cambridge, MA: Massachusetts Institute of Technology, 2003.

[10] J.Y. Cheng, C.A. Ross, E.L. Thomas, H.I. Smith, and G.J. Vancso, *Adv. Mater.* **15** (19), 1599-1602 (2003).

[11] A. Noro, D. Cho, A. Takano, and Y. Matsushita, *Macromolecules* **38**, 4371-4376 (2005).

[12] N.A. Lynd, B.D. Hamilton, and M.A. Hillmyer, *J. Poly. Sci. Poly. Phys.* **45**, 3386-3393 (2007).

[13] J. Acikgoz, Oct. 31, 2008.

[14] R.G.H. Lammertink, M.A. Hempenius, E.L. Thomas, and G.J. Vancso, *J. Poly. Sci. Poly. Phys.* **37**, 1009-1021 (1999).

[15] Y. Ni, R. Rulkens, and I. Manners, *J. Am. Chem. Soc.* **118**, 4102 (1996).

[16] MATLAB code, M.D. Mascaro, March 2009.